BMC Complementary Medicine and Therapies

RESEARCH

Open Access

Evaluation of NTD-O2, a Ghanaian herbal medicine, for onchocerciasis and animal African trypanosomiasis

Barbara Zenabu Anibea[1], Eric Coffie[1], Daniel Moscoh Ayine-Tora[1], Theresa Manful Gwira[2,3] and Dorcas Osei-Safo[1*]

Abstract

Background Herbal medicine remains central to primary healthcare in Ghana due to its accessibility and perceived safety. NTD-O2 is an aqueous herbal formulation derived from *Xylopia aethiopica* fruits and *Bambusa vulgaris* leaves, traditionally used for managing onchocerciasis, a neglected tropical disease (NTD) endemic to the country. This study evaluated the antionchocercal activity of NTD-O2 and assessed isolated compounds from the formulation and its source plants for activity against animal African trypanosomiasis, another prevalent NTD.

Methods Dichloromethane (DCM) and butanol (BuOH) extracts of NTD-O2 were screened in vitro against *Onchocerca ochengi* and *Trypanosoma brucei brucei*. Bioassay-guided fractionation, coupled with spectroscopic and spectrometric techniques, facilitated structural elucidation of isolated compounds. Potential mechanisms of action were explored through in silico molecular docking.

Results Both NTD-O2 extracts achieved 100% inhibition of adult male *O. ochengi* motility. Activity against female worms was moderate (NTD-DCM: 61.0 ± 1.8%; NTD-BuOH: 56.6 ± 4.4%), and weaker against microfilariae (NTD-DCM: 50 ± 0%; NTD-BuOH: 0%). Antitrypanosomal activity was more pronounced, with IC_{50} of 10.68 µg/mL (NTD-DCM) and 9.44 µg/mL (NTD-BuOH), compared to diminazene aceturate (IC_{50} = 0.13 ± 0.02 µg/mL). Cytotoxicity testing on Monkey Kidney Epithelial (LLC-MK2) cells indicated no toxicity. Column chromatography of NTD-BuOH yielded bis(4-methylheptyl) phthalate (1) (IC_{50} = 1.1 ± 0.3 µg/mL) and O2-F3-S (IC_{50} = 100 ± 0.46 µg/mL). By contrast, kaurene diterpenoids from *X. aethiopica* [ent-kaur-16-en-19-oic acid (2), xylopic acid (3), and ent-kaur-16-en-15-one-19-oic acid (4)], along with long-chain carbonyl compounds (5, 6) from *B. vulgaris* were inactive (IC_{50} = > 100 ± 0.46 µg/mL). Molecular modelling results consistently revealed weak binding scores for compounds 2–4 across all three targets (glutathione S-transferase and glutamate-gated chloride channel for onchocerciasis and ornithine decarboxylase for trypanosomiasis).

Conclusion NTD-O2 demonstrated selective antionchocercal and moderate antitrypanosomal activities, validating aspects of its traditional use. However, the presence of phthalate, a compound of known toxicological risks, and the absence of key plant-derived constituents raise concerns about formulation consistency and safety. These findings underscore the need for routine quality control and safety monitoring of herbal medicines to ensure efficacy and public health protection.

*Correspondence:
Dorcas Osei-Safo
dosei-safo@ug.edu.gh

Full list of author information is available at the end of the article

Keywords Herbal medicine, Efficacy, Safety assessment, *Xylopia aethiopica*, *Bambusa vulgaris*, Medicinal plants, Onchocerciasis, Animal African trypanosomiasis, Neglected tropical diseases, Molecular docking

Background

Herbal medicine (HM), rooted in indigenous knowledge and cultural beliefs, has served as the cornerstone of human healthcare for centuries. Today, it remains the primary source of treatment for nearly 80% of the population in developing countries, particularly in rural communities with limited access to conventional medical services [1]. In recent decades, many developed countries have also embraced the use of HM to promote healthier living [2–4]. Despite its widespread use and perception of fewer side effects, HM is usually self-administered and largely unregulated, posing huge safety risks for consumers. To address these concerns and harness their value for achieving universal health coverage, the World Health Organization (WHO) has developed technical guidelines and standards to ensure the safety, efficacy and quality control of HM[5–8].

In Ghana, HM is a significant aspect of cultural heritage, with its development well documented [9–13]. Since 2012, government approval has enabled its integration into the mainstream healthcare system[14], resulting in a wide range of HM products for various conditions. The Ghana Food and Drugs Authority (FDA) oversees their registration and approval based on efficacy, safety, and clinical data. Scientific validation of efficacy claims has supported the rational use of many of these products. However, many FDA-approved products target common ailments such as malaria, anaemia, cough, and asthma, unlike herbal remedies for neglected tropical diseases (NTDs), largely due to lack of access to suitable efficacy testing platforms [12]. As a result, individuals in NTD-endemic communities often rely on unapproved remedies, raising serious concerns about safety and effectiveness and underscoring the urgent need for scientific validation.

Onchocerciasis, commonly known as river blindness, is a parasitic disease caused by the filarial nematode *Onchocerca volvulus* and transmitted through the bite of infected female blackflies (*Simulium*spp.)[15]. The disease is responsible for a range of skin and eye-related morbidities, including irreversible blindness [16]. Despite more than 18 rounds of annual mass drug administration with ivermectin, onchocerciasis remains endemic in several Ghanaian communities [17]. Engagements with the Ghana Federation of Traditional Medicines Practitioners Association (GHAFTRAM) indicate widespread use and high patronage of HM among individuals in NTD-endemic communities [18]. In previous investigation, our research team evaluated the efficacy claims of 15 herbal preparations, several of which demonstrated potential against their target diseases. Interestingly, some of the HMs exhibited significant efficacy (IC_{50} = 5.63–18.71 µg/mL) against animal African trypanosomiasis (AAT), which was not a primary indication [18].

Unlike human trypanosomiasis (sleeping sickness), AAT has received little global attention despite its impact on livestock production, household economies, and human health. Low financial incentives for veterinary drug development have left farmers with few limited treatment options [19]. According to Tweneboah et al.,[20] data on the current situation of AAT in Ghana is scanty, reflecting neglect even at the national level. From our earlier screening, NTD-B4, locally used for schistosomiasis, yielded an isolated compound that was more effective against *Trypanosoma brucei brucei* than the standard antitrypanosomal drug, diminazene aceturate [18]. Another remedy, NTD-O2, traditionally used for the treatment of onchocerciasis, exhibited moderate activity against *Onchocerca ochengi* but greater potency against *T. b. brucei*. Building on these findings, this study investigated NTD-O2 extracts for compounds with both antitrypanosomal and antionchocercal potential. We further examined its source plants, *Xylopia aethiopica* and *Bambusa vulgaris*, for bioactive compounds.

X. aethiopica has been cited in ethnobotanical surveys across West Africa for the management of onchocerciasis and other helminth infections, reflecting its importance in traditional medicine. Pharmacological studies report anti-inflammatory, antimicrobial, and antioxidant properties, but direct evidence of activity against *Onchocerca* species remains limited [21]. In contrast, *Bambusa vulgaris* is more widely studied for general medicinal applications, including antimicrobial, antimalarial, and antioxidant effects, with preliminary studies indicating low acute toxicity [22]. However, no experimental data were found to directly support its use against onchocerciasis or trypanosomiasis. Together, these findings suggest that while both plants possess bioactive constituents of pharmacological interest, their specific roles in managing neglected tropical diseases remain poorly defined and require further validation.

This study is expected to provide a quality assurance framework for NTD-O2 by ensuring its efficacy and safety, thereby enhancing its credibility and ultimately protecting consumers. Specifically, the work aimed to experimentally validate the antionchocercal and antitrypanosomal activities of NTD-O2, isolate and characterize its bioactive constituents alongside those of its constituent plants, and assess their potential mechanisms

of action through complementary in vitro and in silico approaches.

Materials and methods

Herbal medicine and plant materials

NTD-O2 was provided by GHAFTRAM for the study and was obtained as an aqueous herbal formulation prepared from two medicinal plants, the dry fruits of *X. aethiopica* and the fresh leaves of *B. vulgaris*. Dry *X. aethiopica* fruits were sourced from the Nima Market, Accra, and fresh *B. vulgaris* leaves were collected from the University of Ghana campus. Both were identified by Mr. Patrick Ekpe and assigned voucher numbers BZA 001 and BZA 002, respectively, at the Ghana Herbarium, Department of Plant and Environmental Biology, University of Ghana.

Extraction and isolation

Procedure for the herbal medicine (NTD-O2)

NTD-O2 was processed according to the protocol described by Twumasi et al. (2020) [18] with minor modifications. As an aqueous formulation, a total volume of 3.8 L NTD-O2 was subjected to liquid-liquid fractionation in 500 mL aliquots. Each aliquot was transferred into a separatory funnel, and an equal volume of HPLC-grade dichloromethane (DCM) was added. Extraction was performed three times for each aliquot, and the combined organic phases were concentrated to yield the crude extract, NTD-O2-DCM (7 g). This procedure was repeated using n-butanol (n-BuOH) to obtain NTD-O2-BuOH (25 g). The choice of solvents (DCM for nonpolar constituents and BuOH for polar constituents) was intended to achieve effective separation based on polarity. Both extracts were evaluated for their antionchocercal and antitrypanosomal activities. The active extract (NTD-O2-BuOH) was further fractionated sequentially to yield the following fractions: hexane (0.72 g), DCM (0.98 g), ethyl acetate (EtOAc) (2.97 g), and methanol (MeOH) (5.38 g). Each fraction was concentrated under vacuum and refrigerated at 4 °C for approximately 72 h to facilitate the precipitation of solids. The EtOAc fraction yielded a yellow-brown solid (O2-F3-S, 0.5 g), which was purified over a silica gel column (60 g, 130–270 Å mesh, Sigma-Aldrich) eluted with petroleum ether (PE) and EtOAc. The process yielded O2-F3-S (8 mg) and compound 1 (O2-F3-ML, 20 mg).

Procedure for plant materials

Dried powdered fruits of *Xylopia aethiopica* (1 kg) and fresh leaves of *Bambusa vulgaris* (674.0 g) were separately subjected to exhaustive extraction by cold percolation with PE for 72 h. The resulting extracts were concentrated under reduced pressure to yield a brown oily crude extract of *X. aethiopica* (XA/PE, 30.8 g) and a greenish paste of *B. vulgaris* (BL/PE, 10 g). A mass of 10 g of XA/PE was chromatographed on a silica gel column (120 g), eluting sequentially with mixtures of PE and EtOAc in the ratios (v/v): 10:0, 9:1, 8:2, 6:4, 1:1, 0:10, followed by EtOAc: MeOH 9.5:0.5. A total of 315 fractions (20 mL each) were collected and monitored using thin-layer chromatography (TLC). TLC was conducted on silica gel 60 F_{254} (Merck) pre-coated aluminium foil slides, visualized with UV light (254 and 364 nm), and anisaldehyde spray reagent heated to 110 °C.

Fractions with similar TLC profiles were pooled, resulting in 13 combined fractions (F1–F13). After solvent removal under vacuum, fractions F1–F12 were oily, whereas F13 was a powdery solid. Refrigeration of the fractions at 4 °C for approximately 72 h led to the precipitation of colourless crystals of compound 2 (BZA 01, 5 g) from fractions F2–F5. Similarly, fractions F11-F12 yielded another set of colourless crystals, compound 3 (BZA 02, 4.7 g), and fraction F9 produced a greenish powder compound 4 (BZA 05, 200 mg). The *B. vulgaris* extract (BL/PE, 7 g) was subjected to silica gel column chromatography using a protocol similar to that described above. This process yielded two compounds: a white powder, compound 5 (BL 2, 10 mg), and a yellow gum, compound 6 (BL 4, 3 mg).

Structure elucidation techniques

NMR spectra (1D and 2D) were recorded on a Brüker 500 MHz spectrometer in $CDCl_3$, with chemical shifts referenced to tetramethyl silane. LC-MS analysis was performed using an Agilent HPLC system equipped with a Kinetex Core C18 column (2.6 µM, 3 × 50 mm, 100 Å) at 40 °C. The mobile phase consisted of acetonitrile-ethyl acetate (9:1) eluted under gradient conditions at 0.7 mL/min. The injection volume was 2 µL, and the mass spectra were obtained using electrospray ionization (ESI) and atmospheric pressure chemical ionization. GC-MS analysis was conducted on a Perkin Elmer GC Clarus 580 with electron impact ionization at 70 eV and helium gas at 1 mL/min flow rate. National Institute Standard and Technology (NIST) library was used for compound identification [18]. Infrared spectral data were acquired neat on a Perkin Elmer FTIR spectrometer using the attenuated total reflectance technique. MS analyses of the samples were performed using an Agilent 1100 Autosampler instrument with ESI at 3.5 kV and a Thermo Q-Exactive orbitrap instrument. X-ray crystallography measurements were performed on a Brüker ECO D8 diffractometer, with data collection at 296.15 K, the structure was solved using olex2.solve, and refined with ShelXL [23].

Biological assays

In vitro anti-onchocercal assay

Stock solutions (20 mg/mL) of NTD-O2-DCM and NTD-O2-BuOH in DMSO were tested on *O. ochengi* worms and larvae as previously described [18, 24]. Auranofin (10 µM) was used as the positive control, while 2% DMSO served as the negative control. The viability of the adult female worms was evaluated biochemically by visually assessing the percentage inhibition of formazan production after incubating the nodules in 500 µL of 0.5 mg/mL MMT [25]. Loss of the characteristic blue coloration in the worms indicated worm death. A test sample was classified as active if it inhibited more than 90% of female worm motility or formazan production, moderately active if it caused 50–89% inhibition, and inactive if the inhibition was below 50%. Preliminary cytotoxicity studies of the crude extracts were performed on monkey kidney epithelial (LLC-MK2) cells.

In vitro anti-trypanosomal assay

Bloodstream forms of *T. b. brucei* were used in this study due to their similarity to the human-infective forms, *T. b. rhodesiense* and *T. b. gambiense* [26]. The protocol employed is as previously described [18]. Briefly, crude extracts were dissolved in 100% DMSO to make a 20 mg/mL stock, then diluted to 2 mg/mL in sterile distilled water for testing. Compounds 2–6 were prepared in a similar manner. Trypanosome cells in media without treatment served as the negative control, while diminazene aceturate (DA) served as the positive control. Wild-type bloodstream forms of *T. b. brucei*(GuTat 3.1 strain) were cultured in Hirumi's Modified Iscove's Medium-9 (HMI-9)[27], supplemented with 1% penicillin-streptomycin, and 10% heat-inactivated fetal bovine serum (Gibco). The cultures were maintained at 37 °C with 5% CO_2. An Alamar blue assay was used to test the crude extracts and compounds [28]. Serial dilutions (100–0.1953 µg/mL) were prepared in 96-well plates. Log-phase trypanosomes were added, and the plates were incubated for 72 h at 37 °C in 5% CO_2. A final concentration of 44 µM resazurin sodium salt (Sigma-Aldrich) in phosphate-buffered saline was added to each well, and the plates were incubated for an additional 5 h. Fluorescence resulting from the reduction of resazurin to resorufin, which is indicative of cellular metabolic activity, was measured at 570 nm using a Varioskan™ Lux multimode microplate reader (Thermo Fisher Scientific, USA). All experiments were performed in triplicate, with three technical replicates per condition, to ensure statistical reliability.

Statistical analysis

Plate readouts from the Alamar blue assay were evaluated using non-linear regression analysis (log10 inhibitor versus response-variable slope) to assess the growth inhibition. All analyses were performed using GraphPad Prism version 8.0.1. The IC_{50} values of the test samples were determined from three biological replicates, each performed in triplicate.

In silico studies

In silico studies were performed on the fully characterized compounds 2–4 from the current study and a selection of 30 compounds reported from *X. aethiopica* and *B. vulgaris* (Supplementary Information, Table S4) to validate the outcomes of the in vitro antionchocercal and antitrypanosomal assays. These studies included predictions of pharmacodynamics (PD) and pharmacokinetics (PK), as well as molecular modelling of compounds.

Selection of protein targets

For *O. ochengi*, the typical protein targets selected were glutamate-gated chloride ion channel (GluCl) and glutathione S-transferase (GST). GluCl channels are essential for neurotransmission in nematodes, as they regulate chloride ion flow in response to glutamate, thereby controlling muscle movement and overall viability. GluCl is a validated and proven therapeutic target as it is the known molecular target of ivermectin, a frontline drug for onchocerciasis[29, 30]. GST, on the other hand, GST detoxifies host-derived reactive oxygen species, enabling the parasite to evade immune attack and persist within the host [31]. – [32] In the case of *T. b. brucei*, ornithine decarboxylase (ODC) was chosen as the protein target. ODC is a key enzyme in polyamine biosynthesis that catalyzes the decarboxylation of ornithine to produce putrescine, a precursor essential for trypanothione synthesis. Trypanothione is a unique thiol found in trypanosomatids that plays a central role in redox balance and parasite survival, making ODC a critical factor in parasite growth and a validated drug target [33].

Prediction of the PD and PK of the compounds

The SwissADME server was used to predict PD and PK properties of the isolated compounds [34].

Measurement of PK properties and drug-likeness

The SwissADME server was used to determine the physicochemical descriptors of the compounds and to define their PK properties and drug-like nature. The Brain or Intestinal Estimated Permeation (BOILED-Egg) model was employed to intuitively evaluate passive human gastrointestinal absorption (HIA) and blood-brain barrier (BBB) penetration. This model was also used to compute the lipophilicity and polarity of the compounds.

Modelling of compounds

Compounds 2–4 and the 30 selected isolates reported in the literature for *X. aethiopica* and *B. vulgaris*

Table 1 Antionchocercal and antitrypanosomal activities of NTD-O2 extracts

Test sample	Anti-onchocercal activity against *O. ochengi* worms			Antitrypanosomal activity against bloodstream forms *T. b. brucei*
	microfilaria	adult male	adult female	IC_{50} (μg/mL) Mean ± SD
	% inhibition (5 days)		% killing (7 days)	
NTD-O2-DCM	50±0	100±0	61.0±1.8	10.68 ± 2.54
NTD-O2-BuOH	0	100±0	56.6±4.4	9.44 ±1.88
Auranofin		100±0	100±0	
Diminazene aceturate				0.13 ± 0.02

Experiments were done in quadruplicates for adult worms, duplicates for microfilariae, and repeated once

(Supplementary Information, Table S4) were docked to the crystal structures of GST (protein data bank (PDB) ID: 1TU8, resolution 1.80 Å)[32] and GluCl channel (PDB: 3RHW, resolution 3.26 Å), which are protein targets for onchocerciasis [29–32]. Additionally, the compounds were docked against ODC (PDB ID: 1F3T, resolution 2.00 Å)[35], a protein target for trypanosomiasis [33]. The crystal structures of co-crystallized ligands were obtained from PDB [36, 37]. These structures were prepared by removing the co-crystallized ligands and adding hydrogen atoms using the Scigress version FJ 2.6 program. The binding pocket center of GST was identified by fitting the atoms of the co-crystallized ligand 5-hexyl glutathione (x = 2.570, y = 0.814, z = 49.968) with a radius of 10 Å. Similarly, the binding pocket centre of GluCl channel was defined by the position of the atoms of co-crystallized ligand ivermectin (x = 12.675, y = 95.052, z = 24.998) with a radius of 10 Å. The binding pocket centre of ODC was identified by the position of the phosphorus atom of the co-crystallized ligand pyridoxal-5'-phosphate (coordinates: x = 26.206, y = 15.614, z = 3.800) and a radius of 10 Å. To validate the predicted binding modes and relative energies of the ligands, the GoldScore (GS) [38], ChemScore (CS) [39, 40], ChemPLP [41], and Astex statistical potential (ASP) [42] scoring functions were implemented using the GOLD v5.4 software suite.

Results and discussion

In vitro anti-onchocercal and antitrypanosomal activities

The results of the in vitro anti-onchocercal and antitrypanosomal assays are summarized in Table 1. The preliminary cytotoxicity profile of the crude extracts revealed that they were not cytotoxic to LLC-MK2 cells. In primary screens against *O. ochengi*, both crude DCM and butanol extracts of NTD-O2 at 200 μg/mL exhibited complete inhibition (100 ± 0%) of adult male worms. In contrast, the activity against adult female worms was moderate: NTD-O2-DCM achieved 61.0 ± 1.8% inhibition, whereas NTD-O2-BuOH showed 56.6 ± 4.4% inhibition. As strong activity against female worms is a key criterion for advancing to secondary screens, the extracts were not selected for further testing.

Table 2 Antitrypanosomal activities of O2-F3-S and compounds 1–6

Test sample	Antitrypanosomal activity against bloodstream forms of T. b. brucei IC_{50} (μg/mL) Mean ± SD
	Compounds from NTD-O2-BuOH
O2-F3-S	100 ± 0.46
O2-F3-ML (1)	1.1 ± 0.3
	Compounds from *X. aethiopica* and *B. vulgaris*
BZA 01 (2)	> 100 ± 0.46
BZA 02 (3)	ND
BZA 05 (4)	> 100 ± 0.46
BL2 (5)	> 100 ± 0.46
BL4 (6)	> 100 ± 0.46
Diminazene aceturate	0.18 ± 0.01

ND not determined. Calculated adult worm activity responses were performed in quadruplicates, and IC_{50} values represent the mean averages of three biological replicates

Interestingly, the antitrypanosomal assay yielded more positive results, despite the primary target disease for NTD-O2 being onchocerciasis rather than trypanosomiasis. NTD-O2-DCM exhibited an IC_{50} value of 10.68 ± 2.54 μg/mL, while NTD-O2-BuOH was relatively more active against *T. b. brucei* with an IC_{50} of 9.44 ± 1.88 μg/mL. For comparison, the positive control, diminazene aceturate, exhibited an IC_{50} of 0.13 ± 0.02 μg/mL (Table 1).

Although the extracts were less potent than diminazene aceturate, their IC_{50} values suggest the potential for further optimization or use in combination therapies. Based on these findings, NTD-O2-BuOH was prioritized over NTD-O2-DCM for subsequent bioassay-guided fractionation, which yielded O2-F3-S and O2-F3-ML (1). O2-F3-S exhibited limited bioactivity, with an IC_{50} value of 100 ± 0.46 μg/mL. Compound 1, on the other hand, demonstrated significant antitrypanosomal activity, recording an IC_{50} value of 1.1 ± 0.3 μg/mL (Table 2). Its cytotoxicity (CC_{50}) was 100 μg/mL, whereas diminazene aceturate exhibited a CC_{50} of 36 ± 2 μg/mL. In contrast, the standard cytotoxic agent phenylarsine oxide had a CC_{50} of 1.0 ± 0.1 μg/mL, highlighting the relatively moderate cytotoxicity of 1. Based on these values, the

selectivity index (SI) was calculated as 89 ± 25 for compound 1 and 203 ± 22 for diminazene aceturate.

Structure elucidation of isolated compounds

Column chromatographic separation of *X. aethiopica* and *B. vulgaris* extracts afforded compounds 2–6. Compounds 2, 4, 5, and 6 recorded IC_{50} values > 100 ± 0.46 µg/mL and hence, did not demonstrate any antitrypanosomal activity. Compound 3, on the other hand, could not be assayed because of challenges with solubility in DMSO (Table 2).

Compound 1 (O2-F3-ML)

1 was obtained as a yellowish oil with a retention factor (Rf) of 0.75 on TLC developed in a hexane and acetone (7:3) mixture. The infrared (IR) data showed absorptions at 2958 cm-^{1,} 2927 cm^{-1} and 2858 cm^{-1} (C-H), 1726 cm^{-1} (C = O), and 1610 cm^{-1} (aromatic C = C). The ^{1}H-NMR spectrum (Supplementary Information, Figure S1) exhibited a typical AA'BB' system at H-4/H-4' (δ_H 7.53, dd, *J* = 3.3 and 5.7 Hz, 2H) and H-3/H-3' (δ_H 7.70, d, *J* = 3.3 Hz, 2H), supporting an ortho-disubstituted benzene ring with identical substituents in both positions. Signals were observed at δ_H 0.90 (d, *J* = 5.5 Hz, 3H) for the secondary methyl protons H-12/H-12' and δ_H 0.91 (t, *J* = 13.8 Hz, 3H) for the terminal methyl protons H-11/H-11'. A string of multiplets at δ_H 1.31, δ_H 1.35, δ_H 1.42, δ_H 1.68, and δ_H 4.22, was suggestive of methylene groups, with the latter linked to the ester. The ^{13}C NMR and the Distortionless Enhancement by Polarization Transfer (DEPT) 135 spectra (Supplementary Information, Figures S1 and S2) revealed resonances for methyl signals at δ_C 11.1 (C-12/C-12') and δ_C 14.2 (C-11/C-11'), methylene carbon signals at δ_C 23.1 (C-10/C-10'), δ_C 23.9 (C-9/C-9'), δ_C 29.0 (C-8/C-8'), δ_C 30.5 (C-7/C-7'), and an sp^3 methine carbon signal at δ_C 38.9 (C-6/C-6'). The sp^3 oxygenated carbon (C-5/C-5') appeared at δ_C 68.4. Further, there were aromatic methine carbon peaks at δ_C 128.9 (C-4/C-4') and δ_C 131.0 (C-3/C-3') along with a quaternary aromatic carbon peak at δ_C 132.6 (C-2/C-2') and a carbonyl carbon at δ_C 167.9 (C-1/C-1') due to an ester moiety.

Heteronuclear Multiple Bond Correlation (HMBC) spectral data provided correlations between the methyl protons at δ_H 0.90 (H-12) and δ_C 23.1 (C-10), 23.9 (C-9), and 29.0 (C-8). The correlations H-5/C-8 and C-1 established the ester linkage, and H-12/C-6, C-7, C-9, and H-5/C-6 confirmed the branched position of the side chain. The mass spectrum from the GC-MS analysis displayed fragment peaks at m/z 29, 43, 57, 71, 83, 149, 167, and 279, which are characteristic of alkyl phthalates (Supplementary Information, Figure S4). The molecular ion peak appeared at m/z 390 and the base peak at m/z 149, representing a protonated phthalate anhydride. Based on these assignments, the structure of 1 was deduced to be bis(4-methylheptyl) phthalate (Fig. 1).

Phthalates and their derivatives are widely recognized as pervasive environmental contaminants, primarily because of their extensive application in industrial processes, including the manufacture of plastics, personal care products, medical devices, and household items. Their physicochemical properties, particularly their lipophilicity and persistence, promote their accumulation in various environmental matrices, such as soil, water, and air, resulting in widespread human and ecological exposure. Prolonged or excessive exposure to phthalates is associated with a range of adverse health risks in humans. These include endocrine disruption, metabolic disorders, carcinogenic effects, reproductive toxicity,

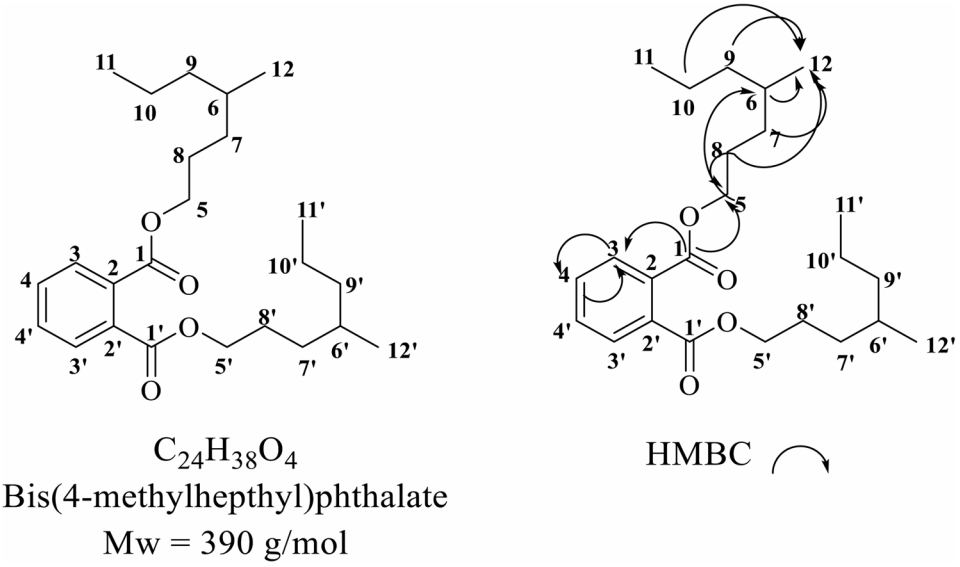

Fig. 1 Chemical structure and HMBC representation of 1 (bis(4-methylhepthyl)phthalate)

and developmental challenges in children [43, 44]. Interestingly, despite their notoriety as synthetic pollutants, some phthalate derivatives have also been detected in natural sources such as plants, bacteria, and fungi, suggesting that some organisms may biosynthesize them naturally. These naturally occurring phthalates exhibit a broad spectrum of biological activities, suggesting their potential pharmacological relevance. Reported bioactivities include antitumor, cytotoxic, allelopathic, larvicidal, antiviral, and anti-inflammatory effects [43]. This dual characteristic of being both environmental toxins and bioactive natural products underscores the complexity of phthalates and highlights the importance of context in evaluating their biological roles.

A review of the literature revealed no documented evidence of bis(4-methylheptyl) phthalate in *X. aethiopica* or *B. vulgaris* or any indication that it is a plant-derived compound [45]. Its presence in NTD-O2 is therefore attributed to leaching from the plastic packaging of the herbal medicine, raising serious safety concerns.

Compound 2 (BZA 01)

2 was obtained as colourless crystals, exhibiting an orange spot upon visualization with anisaldehyde reagent. It showed an Rf value of 0.65 on TLC developed in PE: EtOAc (10:1). The IR spectrum showed characteristic peaks at 1726.56 cm^{-1} for carbonyl and 1687.91 cm^{-1} for unsaturation (C = C).

The ^{13}C NMR and DEPT 135 spectra (Supplementary Information, Figures S5, S6) exhibited 20 carbon signals sorted by the DEPT experiment into 5 quaternary carbons (including a carboxylic carbon at δ_C 185.1 (C-3) and an alkene carbon (C-16) at δ_C 155.8), 3 methine carbons, 2 tertiary methyl carbons and 10 methylene carbons, which were consistent with a kaurenoic acid skeleton. In the ^1H NMR spectrum (Supplementary Information, Figure S7), signals for the olefinic protons H20a (d, δ_H 4.80, 1 H) and H-20b (d, δ_H 4.74, 1 H) and tertiary methyls H-4 (s, δ_H 1.24, 3 H) and H-7 (s, δ_H 0.95, 3-H) supported the presence of kaurenoic acid. HMBC correlations between C-3/H-4, H-5 established the position of the carboxylic acid while the exocyclic alkene was fixed by correlations from C-15, C-16, C-17/H-20a, H-20b.

In addition, the crystal structure revealed an empirical formula of $C_{20}H_{30}O_2$ and M = 302.43 g/mol: $C_{20}H_{30}O_2$ had an orthorhombic, space group $P2_12_12_1$ (no. 19), a = 12.3081(7) Å, b = 23.8205(14) Å, c = 24.0947(14) Å, V = 7064.2(7) $Å^3$, Z = 4, T = 296.15 K, μ(MoKα) = 0.071 mm^{-1}, *Dcalc* = 1.134 g/cm^3, 323,447 reflections measured (4.09° ≤ 2Θ ≤ 57.286°), 18,029 unique (R_{int} = 0.1149, R_{sigma} = 0.0468). The final R_1 was 0.0728 (I >2σ(I)) and wR_2 was 0.1523 (Fig. 2). Consequently, the structure of 2 was determined as ent-kaur-16-en-19-oic acid, previously isolated from *X. aethiopica* [46].

Compound 3 (BZA 02)

3 occurred as colourless crystals. On TLC developed in PE: EtOAc (10:2), the Rf was 0.40 and appeared purple in anisaldehyde spray reagent. The IR spectrum revealed absorption bands of hydroxyl (3280.90 cm^{-1}), carbonyl (1724.65 cm^{-1}) and olefinic C = C stretch (1687.91 cm^{-1}). ^1H and ^{13}C NMR (Supplementary Information, Figures S8, S9) data were similar with those of 2, indicating structural similarities. The significant difference was an additional quaternary carbon peak, δ_C 171.8 (C-21) in compound 3 due to an ester carbonyl peak at δ_C 171.8

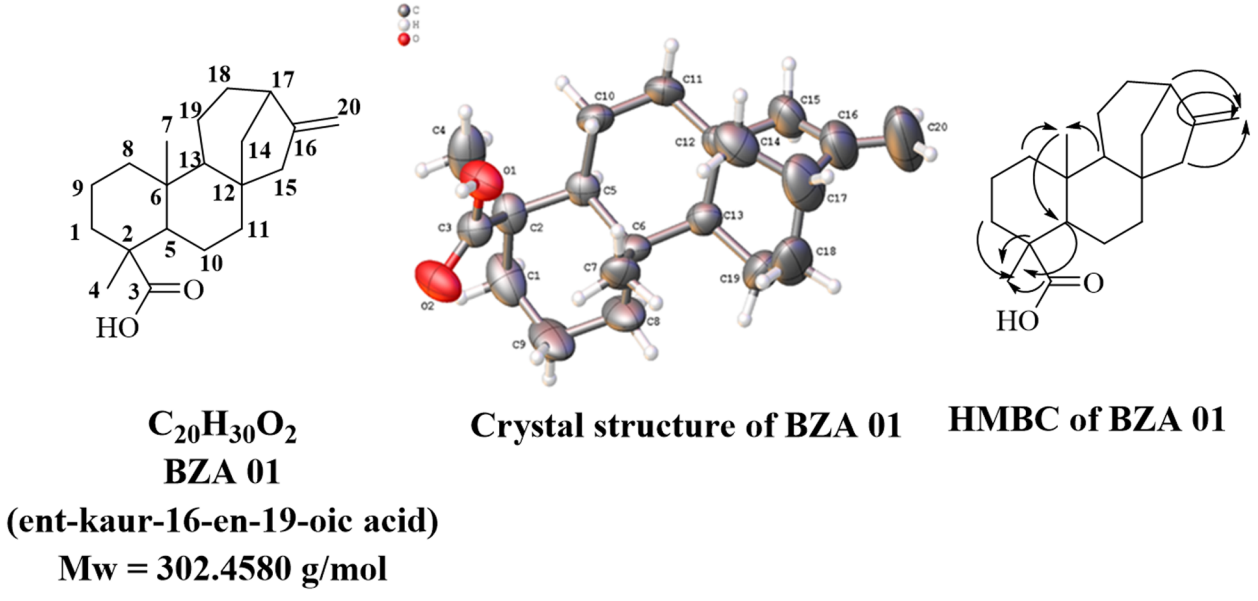

Fig. 2 Chemical and crystal structure, and HMBC representation of 2 (ent-kaur-16-en-19-oic acid)

(C21) and the acetyl carbon at δ_C 21.7 (C-22). The position of the ester group at C-19 was supported by the HMBC correlations of H-20a and H-20b to C-16, C-18 and C-19, suggesting that 3 is xylopic acid, also previously isolated from *X. aethiopica* [47].

X-ray crystallography data gave an empirical formula of $C_{22}H_{32}O_4$ and M = 360.47 g/mol. BZA 02 came out as an orthorhombic shaped crystal with space group $P2_12_12_1$, a = 11.0960(5) Å, b = 11.8948(7) Å, *c* = 14.9745(8) Å, V = 1976.40(18) Å^3, *Z* = 4, *T* = 296.15 K, μ(MoKα) = 0.082 mm-1, Dcalc = 1.211 g/cm^3, 20,732 reflections measured (5.02° ≤ 2Θ ≤ 53.028°), 4083 unique (R_{int} = 0.0979, R_{sigma} = 0.0772) as well as a final R_1 was 0.0460 (I > 2σ(I)) and *w*R_2 was 0.0980 which were used to calculate and confirm the structure of 3 as xylopic acid (Fig. 3).

Compound 4 (BZA 05)

4 was isolated as a fine green powder which exhibited IR and NMR spectra closely resembling those of 2. However, notable differences included a characteristic IR absorption band at 1724.36 cm^{-1}, indicative of a ketone, and a significant downfield shift in the ^{13}C NMR spectrum for carbon C-15, from δ_C 49.1 in 2 to δ_C 210.5 in 4, which is consistent with ketone functionality (Supplementary Information Figure S10). HMBC correlations between C-15 and H-20a, H-20b and H-14 were supportive of the assignment. The proposed structure was corroborated with the MS data analysis which exhibited an M + 1 peak at m/z 317.21 accompanied with fragments at m/z 299.20 and 271.2 (Supplementary Information Figure S11). Hence, the identity 4 was deduced to be ent-kaur-16-en-15-one-19-oic acid [48], with a molar mass of 316 g/mol (Fig. 4).

Compound 5 (BL 2)

5 was isolated as a white powder. Its IR spectrum exhibited characteristic absorption bands for C–H stretching at 2914.8 cm^{-1} and 2848.4 cm^{-1}, a carbonyl group at 1733.8 cm^{-1}, and an olefinic C = C stretch at 1683.9 cm^{-1}. In the ^{13}C NMR spectrum (Supplementary Information, Figure S12), two signals corresponding to carbonyl carbons were observed at δ_C 195.0 (aldehyde) and δ_C 173.7 (ester). Olefinic carbons resonated at δ_C 155.2, 143.6, 134.9, and 124.1. An oxygenated carbon appeared at δ_C 64.1, while the remaining signals, ranging from δ_C 39.3 to δ_C 14.0, indicated the presence of a long alkyl chain. This was further supported by a series of multiplets in the upfield region of the ^{1}H NMR spectrum (δ_H 2.34–0.88). An aldehydic proton was observed at δ_H 9.36, and signals at δ_H 6.44 and 5.12 were attributed to olefinic protons (Supplementary Information, Figure S13).

Compound 6 (BL 2)

6, a yellow gum, showed IR absorption bands at 2916.4 cm^{-1} and 2849 cm^{-1} (C–H stretching) and a carbonyl absorption at 1702.4 cm^{-1}. The ^{13}C NMR spectrum (Supplementary Information, Figure S14) displayed a carbonyl resonance at δ_C 180.5, with additional signals between δ_C 34.5 and 14.5, while the ^{1}H NMR spectrum (Supplementary Information, Figure S15) showed multiplets in the δ_H 2.34–0.88 range. These spectral features are consistent with the structure of a fatty acid.

Molecular modelling

To validate the results of the in vitro antitrypanosomal screening, in silico analysis was conducted to provide further insights into the underlying biological mechanisms involved. Physicochemical descriptors such as

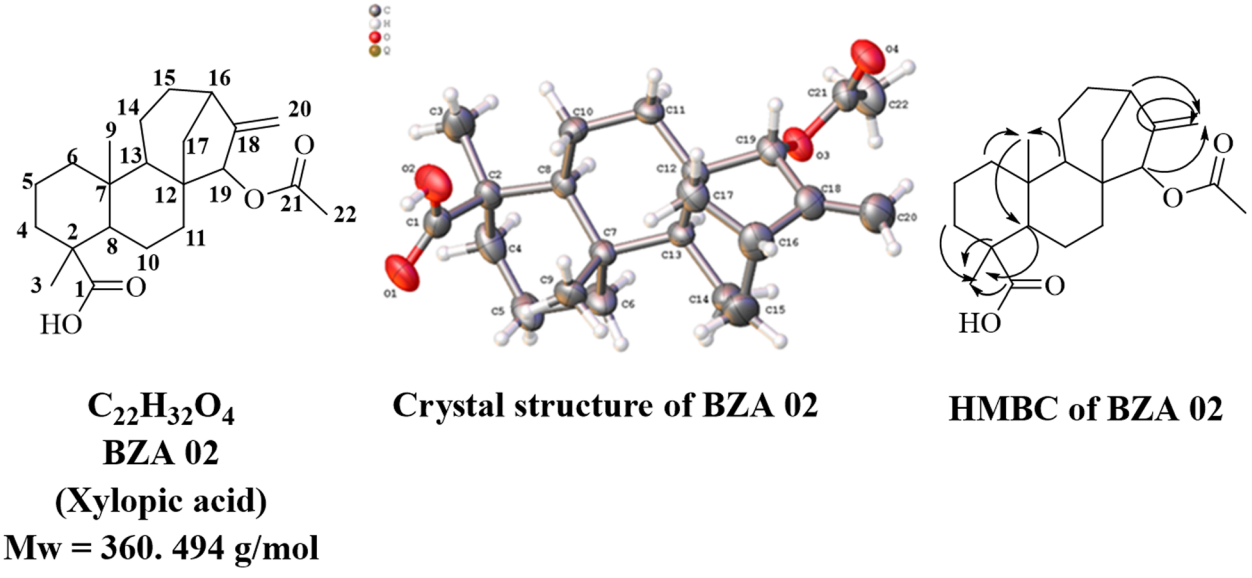

Fig. 3 Chemical and crystal structure, and HMBC representation of 3 (xylopic acid)

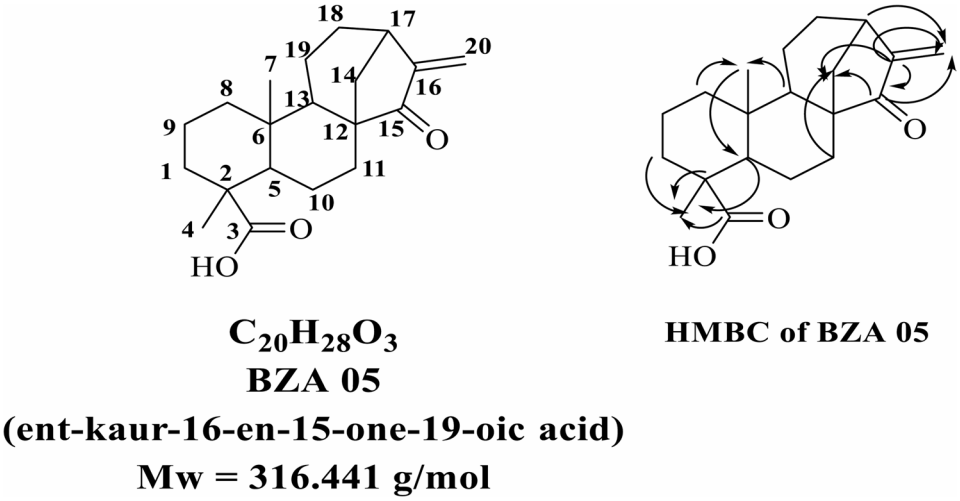

Fig. 4 Chemical structure and HMBC representation of 4 (ent-kaur-16-en-15-one-19-oic acid)

Table 3 Binding score functions of selected compounds docked against GST

Ligand	ASP	PLP	CS	GS
Ivermectin	31.11	66.22	29.8	34.47
3-O-β-sitosterol-β-D-glucopyranoside	35.03	67.74	33.97	49.07
3,4',5-trihydroxy-6",6"-dimethylpyrano (2,3:7,6) flavone	39.3	64.41	30.01	49.67
Tricin 5-O-glucoside	42.52	71.7	26.06	57.98
Farobin B	39.26	67.37	20.8	51.43
Orientin BL	42.25	63.92	21.17	61.15
Kaurenoic acid (2)	23.7	47.38	26.02	37.56
Xylopic acid (3)	23.71	46.02	26.93	41.98
Ent-16-kauren-19-oic acid (4)	22.4	45.36	24.37	39.75

molecular weight (MW) (g/mol), log *P*, hydrogen bond donors (HD), Hydrogen bond acceptors (HA), rotatable bonds (RB), and drug-likeness rules (Lipinski, Ghose, and Veber) were calculated for compounds 2–4 (Supplementary Information, Table S1). The values obtained (HA, HD, RB, log *P* and Lipinski) fell within the drug-like chemical space, and MW was consistent with the known drug space (Supplementary Information, Table S2).

Co-crystallized ligands, including ivermectin (targeting GST) and 5-hexyl glutathione (targeting GluCl channel) for onchocerciasis, as well as pyridoxal-5-phosphate and doxycycline (targeting ODC) for trypanosomiasis, were used as references to predict their functional scores against the respective target sites. Subsequently, compounds 2–4 were docked, alongside selected previously reported metabolites from *X. aethiopica* and *B. vulgaris* (Supplementary Information, Table S4).

Modelling against glutathione S-transferase, GST (Onchocerciasis)

The GST co-crystallized ligand (Supplementary Information, Figure S16) was first docked, yielding root mean square deviation (RMSD) values of ASP = 2.1366, PLP = 5.1415, CS = 1.6223, and GS = 1.9300, with CS and GS showed the strongest predictive power (Supplementary Information, Table S3). Docking revealed that the compounds occupied the hydrophobic binding pockets in plausible orientation. Relative to ivermectin, higher binding affinity scores were observed for 3-O-β-sitosterol-β-D-glucopyranoside, tricin 5-O-glucoside, farobin B, 3,4',5-trihydroxy-6",6"-dimethylpyrano(2,3:7,6) flavone and orientin BL. Notably, orientin BL showed the highest GS score (61.15 vs. 34.47 for ivermectin), while 3-O-β-sitosterol-β-D-glucopyranoside recorded the highest CS score (33.97 vs. 29.8 for ivermectin). In contrast, compounds 2–4 displayed no significant binding (Table 3).

Modelling against glutamate-gated chloride (GluCl) channel (Onchocerciasis)

For the GluCl channel, the co-crystallized ligand (Supplementary Information, Figure S17) produced RMSD values of ASP = 3.4741, PLP = 1.4928, CS = 1.4232, and GS = 1.7654, with PLP and CS providing the best predictive power (Supplementary Information, Table S5). Docking indicated that compounds occupied hydrophilic binding pockets, with 5-hexyl glutathione, achieving the highest scores, followed by 3-O-β-sitosterol´β-D-glucopyranoside and doxycycline. Again compounds 2–4 showed limited binding activity (Table 4 and Supplementary Information, Table S6).

Modelling against ornithine decarboxylase, ODC (Trypanosomiasis)

The co-crystallized ligands, pyridoxal-5-phosphate and doxycycline were docked with ODC (Supplementary Information, Figure S18), yielding RMSD values of ASP = 0.4776, PLP = 1.5959, CS = 6.2696 and GS = 0.6362. In this case, GS and ASP exhibited stronger predictive

Table 4 Binding score functions of selected compounds docked against the glucl channel

Ligand	ASP	PLP	CS	GS
5-hexyl Glutathione	38.41	95.74	41.10	83.81
3-O-β-sitosterol-β-D-glucopyranoside	24.34	82.75	34.38	60.47
Doxycycline	32.38	82.28	20.11	70.06
Kaurenoic acid (2)	15.56	49.31	29.47	33.13
Xylopic acid (3)	16.19	47.27	25.07	35.78
Ent-16-kauren-19-oic acid (4)	16.23	48.17	26.40	36.89

Table 5 Binding score functions of selected compounds docked against ODC

Ligand	ASP	PLP	CS	GS
Pyridoxal-5-phosphate	32.66	51.68	17.92	59.59
Doxycycline	31.04	51.06	29.53	56.27
3-O-β-sitosterol-β-D-glucopyranoside	30.82	65.8	25.8	52.83
3,4′,5-trihydroxy-6″,6″-dimethylpyrano (2,3:7,6) flavone	35.16	60.32	26.34	54.07
Orientin BL	36.18	64.31	19.71	64.74
Kaurenoic acid (2)	22.43	51.33	26.66	34.96
Xylopic acid (3)	22.37	44.07	22.3	40.04
Ent-16-kauren-19-oic acid (4)	21.39	48.6	24.89	33.04

power (Supplementary Information, Table S7). The ligands consistently occupied the hydrophilic binding pockets in plausible binding modes. Consistent with previous observations, compounds 2–4 showed limited binding. In contrast, orientin BL, tricin, 3-O-β-sitosterol ´β-D-glucopyranoside, 3,4′,5-trihydroxy-6″,6″-dimethylpyrano(2,3:7,6) flavone exhibited high binding affinities comparable to pyridoxal-5-phosphate and doxycycline (Table 5, Supplementary Information Table S8).

Overall, the molecular modelling results consistently showed that compounds 2–4 (kaurenoic acid, xylopic acid, and ent-16-kauren-19-oic acid) exhibited limited binding affinity across all three targets (GST, GluCl, and ODC), suggesting a weak likelihood of direct enzyme inhibition as their primary mode of antitrypanosomal action. In contrast, flavonoids such as orientin BL, tricin derivatives, and 3,4′,5-trihydroxy-6″,6″-dimethylpyrano(2,3:7,6)flavone, together with the sterol glycoside 3-O-β-sitosterol-β-D-glucopyranoside, demonstrated consistently high docking scores, in several cases surpassing the reference drugs ivermectin, doxycycline, and pyridoxal-5-phosphate. This comparative trend highlights that while the kaurene diterpenoids (compounds 2–4) may exert biological effects through alternative pathways, the flavonoid and sterol glycoside constituents of *X. aethiopica* and *B. vulgaris* possess stronger multi-target binding potential.

Conclusion

This study experimentally validated aspects of the traditional use of NTD-O2, a Ghanaian herbal medicine, by demonstrating strong antionchocercal activity in male worms, moderate effects against female worms and microfilariae, promising antitrypanosomal activity, and no detectable cytotoxicity. However, the isolation of bis(4-methylheptyl) phthalate, a synthetic plasticizer of known toxicological concern, raises significant concerns about contamination and product authenticity. The absence of comparable bioactivity in the constituent plants, *Xylopia aethiopica* and *Bambusa vulgaris*, further emphasizes the need for rigorous quality assurance.

Complementary in silico studies revealed weak binding affinities for kaurene diterpenoids (compounds 2–4), suggesting limited likelihood of direct enzyme inhibition, whereas flavonoids and sterol glycosides reported in the source plants exhibited consistently strong multi-target binding, in some cases surpassing reference drugs. These findings suggest that while certain phytochemicals have genuine pharmacological relevance, the observed efficacy of NTD-O2 may not reliably reflect its declared plant origins.

Overall, the findings highlight a dual imperative: to validate the therapeutic potential of Ghanaian herbal medicines through integrated in vitro, in silico, and in vivo approaches, while simultaneously instituting robust quality control measures to eliminate contaminants and ensure consumer safety.

Abbreviations

AAT	Animal African trypanosomiasis
ASP	Astex statistical potential
CS	ChemScore
DA	Diminazene aceturate
DEPT	Distortionless Enhancement by Polarization Transfer
GHAFTRAM	Ghana Federation of Traditional Medicines Practitioners Association
FDA	Ghana Food and Drugs Authority
GluCl	Glutamate-gated chloride channel
GST	Glutathione S-transferase
GS	GoldScore
HM	Herbal medicine
HMBC	Heteronuclear Multiple Bond Correlation
HIA	Human gastrointestinal absorption
NTDs	Neglected tropical diseases
ODC	Ornithine decarboxylase
PD	Pharmacodynamics
PK	Pharmacokinetics
PDB	Protein Data Bank
RMSD	Root mean square deviation
SI	Selective index
TLC	Thin Layer Chromatography
WHO	World Health Organization

Supplementary Information

The online version contains supplementary material available at https://doi.org/10.1186/s12906-025-05208-y.

Supplementary Material 1.

Acknowledgements

The authors express their gratitude to the Department of Chemistry, University of Ghana, for NMR and X-ray data acquisition and New Zealand eScience Infrastructure (NeSI) high-performance computing facilities as part of this research funded jointly by the collaborating institutions and through

the Ministry of Business, Innovation and Employment Research Infrastructure program. URL: https://www.nesi.org.nz. The Trypanosoma brucei brucei cell line (GUTat 3.1 strain) was originally obtained from the Department of Parasitology, Noguchi Memorial Institute for Medical Research, University of Ghana.

Authors' contributions
BZA : Data acquisition and analysis; Writing – original draft, revision and final approval.**EC** : Data acquisition and analysis; Writing – revision and final approval**DM** : Supervision, Data acquisition and analysis; Writing –revision and final approval**TMG** : Supervision, Data acquisition and analysis; Writing –revision and final approval**DOS** : Funding acquisition, Conceptualization, Supervision, Data analysis. Writing – original draft, revision and final approval.

Funding
This research was supported by Worldwide Universities Network Research Development Fund 2017 from the Worldwide Universities Network (UK) and grant number 18–191 RG/CHE/AF/AC_G - FR3240303659 from The World Academy of Sciences.

Data availability
The dataset supporting the conclusions of this article is included within the article and its additional file.

Declarations

Ethics approval and consent to participate
Not applicable.

Consent for publication
Not applicable.

Competing interests
The authors declare no competing interests.

Author details
[1]Department of Chemistry, University of Ghana, Accra, Ghana
[2]West African Centre for Cell Biology of Infectious Pathogens, University of Ghana, Accra, Ghana
[3]Department of Biochemistry, Cell and Molecular Biology, University of Ghana, Accra, Ghana

Received: 22 July 2025 / Accepted: 1 December 2025
Published online: 09 December 2025

References

1. Hoenders R, Ghelman R, Portella C, Simmons S, Locke A, Cramer H, Gallego-Perez D, Jong M. A review of the WHO strategy on traditional, complementary, and integrative medicine from the perspective of academic consortia for integrative medicine and health. Front Med. 2024;11:1395698. https://doi.org/10.3389/fmed.2024.1395698.
2. Bodeker G, Kronenberg F. A public health agenda for traditional, complementary, and alternative medicine. Am J Public Health. 2002;92(10):1582–91.
3. Ernst E. Prevalence of use of complementary/alternative medicine: a systematic review. Bull World Health Organ. 2000;78(2):252–7.
4. Nissen N. Practitioners of Western herbal medicine and their practice in the UK: beginning to sketch the profession. Complement Ther Clin Pract. 2010;16(4):181–6.
5. Flynn MAT, Maloff DA, Maloff B, Mutasingwa D, Wu M, Ford C, et al. Reducing obesity and related chronic disease risk in children and youth: a synthesis of evidence with 'best practice' recommendations. Obes Rev. 2006;6(1):7–16.
6. Akerele O. WHO's traditional medicine programme: progress and perspectives. WHO Chron. 1984;38(2):76–81.
7. World Health Organization (WHO). WHO traditional medicine strategy: 2014–2023. Geneva: WHO; 2013. Report No.
8. World Health Organization. WHO traditional medicine strategy 2002–2005. Geneva, Switzerland: World Health Organization; 2002. Global review.
9. Twumasi PA. History of pluralistic medical systems: a sociological analysis of the Ghanaian case. Issue. 1979;9(3):29–34.
10. Essegbey GO, Awuni S. Herbal medicine in the informal sector of Ghana. In: Kraemer-Mbula E, Wunsch-Vincent S, editors. The informal economy in developing nations: hidden engine of innovation? Cambridge: Cambridge University Press; 2016. pp. 194–231.
11. Addae-Mensah I. Herbal medicine: does it have a future in Ghana? 1975.
12. Mintah SO, Archer M-A, Asafo-Agyei T, Ayertey F, Aboagye-Antwi P, Boamah D, et al. Medicinal plant use in ghana: advancement and challenges. Am J Plant Sci. 2022;13(3):316–58.
13. Ministry of Health (MOH). Policy guidelines on traditional medicine development: traditional medicine policy. Accra: Ministry of Health; 2005. pp. 1–15.
14. Owoahene-Acheampong EVAS. Recognition and integration of traditional medicine in Ghana: a perspective. Res Rev. 2010;26(2):1–17.
15. Crawford KE, Hedtke SM, Doyle SR, Kuesel AC, Armoo S, Osei-Atweneboana M, Grant WN. Genome-based tools for onchocerciasis elimination: utility of the mitochondrial genome for delineating *Onchocerca volvulus* transmission zones. Int J Parasitol. 2024;54(3–4):171–83. https://doi.org/10.1016/j.ijpara.2023.11.002.
16. Brattig NW, Cheke RA, Garms R. Onchocerciasis (river blindness) – more than a century of research and control. Acta Trop. 2021;218:105677.
17. Chikezie FM, Veriegh FBD, Armoo S, Boakye DA, Taylor M, Osei-Atweneboana MY. . Ongoing transmission of onchocerciasis in the Pru District of Ghana after two decades of mass drug administration with ivermectin and comparative identification of members of the *Simulium damnosum* complex using cytological and morphological techniques. Parasit Vectors. 2024;17(1):394.
18. Twumasi EB, Akazue PI, Kyeremeh K, Gwira TM, Keiser J, Cho-Ngwa F, et al. Antischistosomal, antionchocercal and antitrypanosomal potentials of some Ghanaian traditional medicines and their constituents. PLoS Negl Trop Dis. 2020;14(12):e0008919.
19. Pereira SH, Alves FP, Teixeira SMR. Animal trypanosomiasis: challenges and prospects for new vaccination strategies. Microorganisms. 2024;12(12):2575. https://doi.org/10.3390/microorganisms12122575.
20. Tweneboah A, Rosenau J, Addo KA, Addison TK, Ibrahim MAM, Weber JS, et al. The transmission of animal African trypanosomiasis in two districts in the forest zone of Ghana. Am J Trop Med Hyg. 2024;110(6):1127–36.
21. Katawa G, Ataba E, Ritter M, Amessoudji OM, Awesso ER, Tchadié PE, et al. Anti-Th17 and anti-Th2 responses effects of hydro-ethanolic extracts of *Aframomum melegueta*, *Khaya senegalensis* and *Xylopia aethiopica* in hyper-reactive onchocerciasis individuals' peripheral blood mononuclear cells. PLoS Negl Trop Dis. 2022;16:e0010341.
22. Akhtar J, Patowary L. *Bambusa vulgaris*: a comprehensive review of its traditional uses, phytochemicals and pharmacological activities. Sciences of Phytochemistry. 2022;1:11–21.
23. Sheldrick GM. Crystal structure refinement with SHELXL. Acta Crystallogr C Struct Commun. 2015;71:3–8.
24. Gyapong JO, Kumaraswami V, Biswas G, Ottesen EA. Treatment strategies underpinning the global programme to eliminate lymphatic filariasis. Expert Opin Pharmacother. 2005;6(2):179–200.
25. Nyongbela KD, Samje M, Awantu AF, Tiku TE, Cho-Ngwa F. Evaluation of anti-onchocercal activity of pseudopalmatine, a quaternary Protoberberine alkaloid of *Enantia Chlorantha* (Syn. *Annickia Chlorantha*). J Cameroon Acad Sci. 2019;14(3):171. https://doi.org/10.4314/jcas.v14i3.1.
26. Neuberger A, Meltzer E, Leshem E, Dickstein Y, Stienlauf S, Schwartz E. The changing epidemiology of human African trypanosomiasis among patients from nonendemic countries – 1902–2012. PLoS ONE. 2014;9(2):e88647.
27. Hirumi H, Hirumi K. Axenic culture of African trypanosome bloodstream forms. *Parasitol Today*. 1994;10(2):80–4.
28. Raz B, Iten M, Grether-Bühler Y, Kaminsky R, Brun R. Alamar blue assay to determine drug sensitivity of African trypanosomes (*T.b. Rhodesiense* and *T.b. gambiense*) in vitro. Acta Trop. 1997;68:139–47.
29. Glendinning SK, Buckingham SD, Sattelle DB, Wonnacott S, Wolstenholme AJ. Glutamate-gated chloride channels of *Haemonchus contortus* restore drug sensitivity to ivermectin-resistant *Caenorhabditis elegans*. PLoS One. 2011;6(7):e22390.
30. Atif M, Estrada-Mondragon A, Nguyen B, Lynch JW, Keramidas A. Effects of glutamate and Ivermectin on single glutamate-gated chloride channels of the parasitic nematode *H. contortus*. PLoS Pathog. 2017;13(10):e1006663.
31. Salinas G, Taylor DW. Molecular characterisation and localisation of an *Onchocerca volvulus* p-class glutathione-S-transferase. Mol Biochem Parasitol. 1994;66:10.
32. Perbandt M, Hoppner J, Betzel C, Walter RD, Liebau E. Structure of the major cytosolic glutathione S-transferase from the parasitic nematode *Onchocerca volvulus*. J Biol Chem. 2005;280(13):12630–6.

33. Jackson LK, Babbitt HB, Osterman AL, Goldsmith EJ, Phillips MA. Altering the reaction specificity of eukaryotic ornithine decarboxylase. Biochemistry. 2000;39(37):11.
34. Daina A, Michielin O, Zoete V. Swissadme: a free web tool to evaluate pharmacokinetics, drug-likeness and medicinal chemistry friendliness of small molecules. Sci Rep. 2017;7:42717.
35. Gladkova ED, Nechepurenko IV, Bredikhin RA, Chepanova AA, Zakharenko AL, Luzina OA, et al. The first berberine-based inhibitors of tyrosyl-DNA phosphodiesterase 1 (Tdp1), an important DNA repair enzyme. Int J Mol Sci. 2020;21(19):7162. https://doi.org/10.3390/ijms21197162.
36. Berman H, Henrick K, Nakamura H. Announcing the worldwide protein data bank. Nat Struct Biol. 2003;10(12):1.
37. Kitchen DB, Decornez H, Furr JR, Bajorath J. Docking and scoring in virtual screening for drug discovery: methods and applications. Nat Rev Drug Discov. 2004;3(11):935–49.
38. Jones G, Willett P, Glen RC, Leach AR, Taylor R. Development and validation of a genetic algorithm for flexible docking. Mol Biol. 1997;267:22.
39. Eldridge MD, Murray CW, Auton TR, Paolini GV, Mee RP. Empirical scoring functions: the development of a scoring function to estimate the binding affinity of ligands in receptor complexes. J Comput Aided Mol Des. 1997;11:21.
40. Miller PS, Smart TG. Binding, activation and modulation of Cys-loop receptors. Trends Pharmacol Sci. 2010;31(4):161–74.
41. Korb O, Stützle T, Exner TE. Empirical scoring functions for advanced protein-ligand docking with PLANTS. J Chem Inf Model. 2009;49(1):84–96.
42. Mooij WT, Verdonk ML. General and targeted statistical potentials for protein-ligand interactions. Proteins. 2005;61(2):272–87.
43. Yasmin F, Nazli Z-i-H, Shafiq N, Aslam M, Bin Jardan YA, Nafidi H-A, et al. Plant-based bioactive phthalates derived from *Hibiscus rosa-sinensis*: as in vitro and in silico enzyme inhibition. ACS Omega. 2023;8(36):32677–89.
44. Omidpanah S, Saeidnia S, Saeedi M, Hadjiakhondi A, Manayi A. Phthalate contamination of some plants and herbal products. Bol Latinoam Caribe Plant Med Aromat. 2018;17(1):61–7.
45. Huang L, Zhu X, Zhou S, Cheng Z, Shi K, Zhang C, Shao H. Phthalic acid esters: natural sources and biological activities. Toxins. 2021;13(7):495.
46. Somova LI, Sinyangwe FO, Moodley K, Govender Y. Cardiovascular and diuretic activity of kaurene derivatives of *Xylopia aethiopica* and *Alepidea amatymbica*. J Ethnopharmacol. 2021;77:10.
47. Soh D, Ernestine N, Tchana Satchet EM, Defokou UD, Schneider B, Giovanni V, et al. Antiproliferative activity of semisynthetic xylopic acid derivatives. Nat Prod Res. 2022;36(5):1288–95.
48. Fetse J, Kofie W, Adosraku R. Ethnopharmacological importance of *Xylopia aethiopica* (Dunal) A. Rich (Annonaceae) – A review. Br J Pharm Res. 2016;11(1):1–21. https://doi.org/10.9734/BJPR/2016/24746.

Publisher's Note